

Two-loop leading-colour QCD helicity amplitudes for two-photon plus jet production at the LHC

Herschel A. Chawdhry,^a Michał Czakon,^b Alexander Mitov,^c Rene Poncelet^c

^a*Rudolf Peierls Centre for Theoretical Physics, Clarendon Laboratory, University of Oxford, Oxford OX1 3PU, United Kingdom*

^b*Institut für Theoretische Teilchenphysik und Kosmologie, RWTH Aachen University, D-52056 Aachen, Germany*

^c*Cavendish Laboratory, University of Cambridge, Cambridge CB3 0HE, United Kingdom*

ABSTRACT: We calculate the complete set of two-loop leading-colour QCD helicity amplitudes for $\gamma\gamma j$ -production at hadron colliders. Our results are presented in a compact, fully-analytical form.

¹Preprint: OUTP-21-06P, Cavendish-HEP-21/05, P3H-21-014, TTK-21-09

Contents

1	Introduction	1
2	Calculation	2
3	Results	5
4	Conclusions	7
A	Benchmark numerical results for the finite remainder	9
B	Renormalisation constants	9

1 Introduction

Multi-loop scattering amplitudes are core ingredients in high-precision perturbative calculations in Quantum Field Theory. The complexity of these amplitudes rapidly increases with the number of loops, external legs, and kinematic scales in a process. Scattering amplitudes in Quantum Chromodynamics (QCD) and Electroweak theory are of particular interest due to their central role in theoretical predictions for processes at the Large Hadron Collider (LHC).

The last few years have seen many advances in the calculation of multi-loop integrals and amplitudes [1–30]. Two-loop 5-point amplitudes are at the frontier of current amplitude calculations and have been the subject of particularly intense research [31–46]. That research has notably led to the calculation of the 2-loop QCD leading-colour amplitude for $q\bar{q} \rightarrow \gamma\gamma\gamma$ [40, 42, 43], which in turn has enabled, for the first time, the computation of the Next-to-Next-to-Leading-Order (NNLO) QCD corrections for a $2 \rightarrow 3$ process [40, 47].

In this work we calculate the complete set of 2-loop leading-colour QCD helicity amplitudes for the processes $q\bar{q} \rightarrow g\gamma\gamma$ and $qg \rightarrow q\gamma\gamma$. These amplitudes enable the calculation of the double-virtual QCD corrections to $\gamma\gamma j$ production at hadron colliders. They are also required, alongside the recently-calculated 3-loop QCD amplitude $q\bar{q} \rightarrow \gamma\gamma$ [48], to calculate the N³LO QCD correction to $\gamma\gamma$ production, which is an important background for inclusive Higgs boson measurements at the LHC.

This paper is organised as follows. Our calculation is described in Section 2, including details of the infrared subtraction and helicity projections. Our results are presented in Section 3 and our conclusions are presented in Section 4. Some benchmark results are given in appendix A. The analytic results derived in this paper are rather compact and are available for download in electronic form.

2 Calculation

We consider the partonic processes

$$\begin{aligned} q_c^{h_1}(p_1)\bar{q}_{c'}^{h_2}(p_2) &\rightarrow g_a^{h_3}(p_3)\gamma^{h_4}(p_4)\gamma^{h_5}(p_5), \\ q_c^{h_1}(p_1)g_a^{h_2}(p_2) &\rightarrow q_{c'}^{h_3}(p_3)\gamma^{h_4}(p_4)\gamma^{h_5}(p_5), \end{aligned} \quad (2.1)$$

where $h_i \in \{+, -\}$ denotes the helicity of the i^{th} parton, $i = 1, \dots, 5$. The indices c and c' denote the colours of the quarks while the index a denotes the colour of the gluon. The momenta p_1 and p_2 are incoming while p_3 , p_4 , and p_5 are outgoing. All partons are massless and on-shell: $p_i^2 = 0$. Momentum conservation and on-shell conditions leave five independent parity-even Lorentz invariants $s_{ij} = (p_i + p_j)^2$ and one parity-odd invariant $\text{tr}_5 = 4i\varepsilon_{p_1 p_2 p_3 p_4}$. We choose the following set of variables to parametrise the amplitudes:

$$x = \{s_{12}, s_{23}, s_{34}, s_{45}, s_{51}, \text{tr}_5\}. \quad (2.2)$$

All other Lorentz invariants can be expressed in terms of this set in the following way:

$$s_{13} = s_{12} - s_{23} - s_{45}, \quad (2.3)$$

$$s_{14} = -s_{51} + s_{23} + s_{45}, \quad (2.4)$$

$$s_{24} = s_{51} - s_{23} + s_{34}, \quad (2.5)$$

$$s_{25} = s_{12} - s_{15} - s_{34}, \quad (2.6)$$

$$s_{35} = s_{12} - s_{34} - s_{45}. \quad (2.7)$$

The physical scattering region satisfies [7] the following equations:

$$s_{12} > 0, \quad s_{12} \geq s_{34}, \quad s_{45} \leq s_{12} - s_{34}, \quad s_{23} > s_{12} - s_{45}, \quad s_{51}^- \leq s_{51} \leq s_{51}^+, \quad (\text{tr}_5)^2 < 0, \quad (2.8)$$

with

$$\begin{aligned} (\text{tr}_5)^2 &= s_{12}^2(s_{23} - s_{51})^2 + (s_{23}s_{34} + s_{45}(s_{34} + s_{51}))^2 - \\ &2s_{12}(s_{23}^2s_{34} + s_{23}s_{34}s_{45} - s_{23}(s_{34} + s_{45})s_{51} + s_{45}s_{51}(s_{34} + s_{51})), \end{aligned} \quad (2.9)$$

and

$$\begin{aligned} s_{51}^\pm &= \frac{1}{(s_{12} - s_{45})^2} \left(s_{12}^2 s_{23} + s_{12} s_{34} s_{45} - s_{23} s_{34} s_{45} - s_{34} s_{45}^2 - \right. \\ &\left. s_{12} s_{23} (s_{34} + s_{45}) \pm 2\sqrt{s_{12} s_{23} s_{34} s_{45} (s_{45} + s_{23} - s_{12})(s_{45} + s_{34} - s_{12})} \right). \end{aligned} \quad (2.10)$$

The UV-renormalised amplitude for these processes is denoted by:

$$\mathcal{M}(\alpha_s)_{cc'a}^{f, h_1 h_2 h_3 h_4 h_5}(x) = \mathbf{T}_{cc'}^a \mathcal{M}(\alpha_s)^{f, h_1 h_2 h_3 h_4 h_5}(x) \equiv \mathbf{T}_{cc'}^a \mathcal{M}^{f, \bar{h}}, \quad (2.11)$$

where we have factored out the tree-level colour structure. The index f denotes the flavour structure, which is $f = q\bar{q}$ and $f = qg$ for the $q\bar{q}$ - and qg -initiated processes respectively. We

summarise the helicity configuration by $\bar{h} = \{h_1, h_2, h_3, h_4, h_5\}$ and suppress the kinematic dependence for brevity. The amplitude can be expanded in α_s :

$$\mathcal{M}^{f,\bar{h}} = \sqrt{\alpha_s 4\pi} \left(\mathcal{M}^{f,\bar{h}(0)} + \left(\frac{\alpha_s}{4\pi}\right) \mathcal{M}^{f,\bar{h}(1)} + \left(\frac{\alpha_s}{4\pi}\right)^2 \mathcal{M}^{f,\bar{h}(2)} + \mathcal{O}(\alpha_s^3) \right). \quad (2.12)$$

The UV-renormalised amplitude $\mathcal{M}^{\bar{h}}$ is related to the bare amplitude computed in $d = 4 - 2\varepsilon$ dimensions $\mathcal{M}^{\bar{h},B}$ through:

$$\mathcal{M}^{f,\bar{h}}(\alpha_s) = \left(\frac{\mu^2 e^{\gamma_E}}{4\pi} \right)^{-2\varepsilon} \mathcal{M}^{f,\bar{h},B}(\alpha_s^0). \quad (2.13)$$

The bare coupling α_s^0 is renormalised in the $\overline{\text{MS}}$ scheme according to:

$$\alpha_s^0 = \left(\frac{e^{\gamma_E}}{4\pi} \right)^\varepsilon \mu^{2\varepsilon} Z_{\alpha_s} \alpha_s. \quad (2.14)$$

The renormalisation constant Z_{α_s} is given in appendix B.

The IR divergences of the UV-renormalised amplitude can be factorised by means of the so-called \mathbf{Z} operator:

$$\mathcal{M}^{f,\bar{h}} = \mathbf{Z}^f \mathcal{F}^{f,\bar{h}}. \quad (2.15)$$

We define \mathbf{Z}^f in the $\overline{\text{MS}}$ scheme. Its explicit expression through 2 loops in QCD is given in appendix B. We note that eq. (2.15) completely specifies the finite remainder $\mathcal{F}^{f,\bar{h}}$.

Once the \mathbf{Z}^f factor, the finite remainder \mathcal{F} , and the amplitude \mathcal{M} have been expanded in powers of $\alpha_s/(4\pi)$, eq. (2.15) reduces to ¹

$$\mathcal{M}^{f,\bar{h},(0)} = \mathcal{F}^{f,\bar{h}(0)}, \quad (2.16)$$

$$\mathcal{M}^{f,\bar{h},(1)} = \mathbf{Z}^{f,(1)} \mathcal{M}^{f,\bar{h}(0)} + \mathcal{F}^{f,\bar{h}(1)}, \quad (2.17)$$

$$\mathcal{M}^{f,\bar{h},(2)} = \mathbf{Z}^{f,(2)} \mathcal{M}^{f,\bar{h}(0)} + \mathbf{Z}^{f,(1)} \mathcal{F}^{f,\bar{h}(1)} + \mathcal{F}^{f,\bar{h}(2)}. \quad (2.18)$$

The amplitude can be decomposed in terms of colour factors and the electric charges Q_q and Q'_q of, respectively, the external quark q and the quarks q' propagating in loops. The tree-level and 1-loop results will be given in sec. 3 below. The complete 2-loop finite remainder, including the non-planar topologies, can be decomposed as follows:

$$\mathcal{F}^{(2)} = Q_q^2 \mathcal{F}^{(2),Q_q^2} + Q_q Q_{l,1} \mathcal{F}^{(2),Q_q Q_{q'}} + Q_{l,2} \mathcal{F}^{(2),Q_{q'}^2}, \quad (2.19)$$

where we have introduced the abbreviation $Q_{l,n} = \sum_{q'} Q_{q'}^n$.

In this work we only calculate the contributions from planar diagrams. To single them out, we expand the charge structures in the large- N_c limit

$$\begin{aligned} \mathcal{F}^{(2),Q_q^2} &= N_c^2 \left(\mathcal{F}^{(2),Q_q^2,N_c^2} + \frac{n_f}{N_c} \mathcal{F}^{(2),Q_q^2,n_f} + \mathcal{O}\left(\frac{1}{N_c}\right) \right), \\ \mathcal{F}^{(2),Q_q Q_{q'}} &= N_c \left(\mathcal{F}^{(2),Q_q Q_{q'},N_c} + \mathcal{O}\left(\frac{1}{N_c}\right) \right), \\ \mathcal{F}^{(2),Q_{q'}^2} &= N_c \left(\mathcal{F}^{(2),Q_{q'}^2,N_c} + \frac{n_f}{N_c} \mathcal{F}^{(2),Q_{q'}^2,n_f} + \mathcal{O}\left(\frac{1}{N_c}\right) \right), \end{aligned} \quad (2.20)$$

¹The α_s expansion of $\mathcal{F}^{f,\bar{h}}$ is analogous to the one in eq. (2.12).

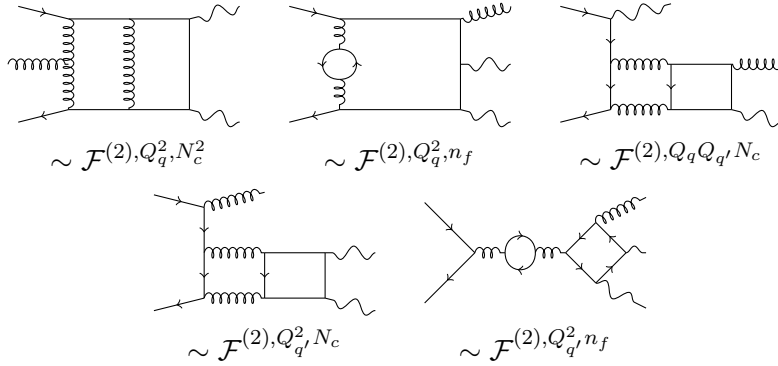


Figure 1. Representative two-loop diagrams for the contributing colour/charge coefficients.

where the $\mathcal{O}(1/N_c)$ terms receive contributions from non-planar diagrams. Furthermore, the contributions $\mathcal{F}^{(2), Q_{q'}^2, N_c}$ and $\mathcal{F}^{(2), Q_q Q_{q'}, N_c}$ also have contributing non-planar diagrams and are not considered in this work. The explicit expressions for the 2-loop finite remainders are given in sec. 3 below.

The partonic process $q\bar{q} \rightarrow g\gamma\gamma$ given in eq. (2.1) has three independent helicities. We choose the following set:

$$\mathcal{F}^{q\bar{q}, \{+----\}} \quad , \quad \mathcal{F}^{q\bar{q}, \{+-+--\}} \quad \text{and} \quad \mathcal{F}^{q\bar{q}, \{+---+\}} \quad . \quad (2.21)$$

All other helicity configurations can be obtained from the above three by conjugation and/or permutation of the external momenta. We note that the helicity amplitudes $\mathcal{F}^{q\bar{q}, \{+----\}}$, $\mathcal{F}^{q\bar{q}, \{++++--\}}$ and $\mathcal{F}^{q\bar{q}, \{+-++++\}}$ vanish at tree-level. For this reason they do not contribute to the 2-loop squared matrix element and enter NNLO QCD computations only through the 1-loop-squared matrix element.

The partonic process $qg \rightarrow q\gamma\gamma$ specified in eq. (2.1) can similarly be expressed in terms of three independent helicities, and the remaining helicities can be obtained by conjugation and/or permutation of external legs. Unlike the $q\bar{q}$ initiated process, however, the qg one involves crossings between the initial and the final states. Such crossings involve a practical complication related to the nature of the pentagon functions [49] used to express these amplitudes; it originates in the fact that these functions' representation does not allow crossings between the initial and final states in the course of their numerical evaluation. For this reason, we have computed analytically six helicities from which all remaining ones can be obtained by crossing final-state momenta only:

$$\begin{aligned} & \mathcal{F}^{qg, \{+-+--\}} \quad , \quad \mathcal{F}^{qg, \{++++--\}} \quad \text{and} \quad \mathcal{F}^{qg, \{+++++-\}} \quad , \\ & \mathcal{F}^{qg, \{+-++++\}} \quad , \quad \mathcal{F}^{qg, \{++++++\}} \quad \text{and} \quad \mathcal{F}^{qg, \{+-++++\}} \quad . \end{aligned} \quad (2.22)$$

All other helicities for this process can be obtained from the above six by conjugation and/or permutation of final-state momenta.

Just as in our recent 3-photon calculation [43], we have decomposed the amplitudes using the helicity projection method proposed in ref. [50]. The construction of the gluon/photon polarization vector follows closely ref. [43]. The fermion projector in our previous work was designed with the permutation symmetry of the final-state photons in mind. The partonic processes considered here are less symmetric and thus we consider a simpler projector. In the case of the $q\bar{q} \rightarrow g\gamma\gamma$ partonic process, the fermionic line is projected by considering the following trace in spin space:

$$\mathcal{M} = \bar{v}(p_2, h_2)\Gamma u(p_1, h_1) = \text{Tr}\left\{(u \otimes \bar{v})\Gamma\right\}, \quad (2.23)$$

where Γ represents the spinor-stripped amplitude. The density operator $u \otimes \bar{v}$ can be rearranged to

$$(u \otimes \bar{v})_{\alpha\beta} = \frac{1}{\bar{u}Nv}[(u \otimes \bar{u})N(v \otimes \bar{v})]_{\alpha\beta}, \quad (2.24)$$

with any N for which $\bar{u}Nv \neq 0$. We choose here $N = \not{p}_3$. The projectors for the $qg \rightarrow q\gamma\gamma$ process are obtained from those for $q\bar{q} \rightarrow g\gamma\gamma$ by applying the crossing $p_2 \leftrightarrow p_3$.

The amplitudes are expressed in terms of a minimal basis of irrational functions by means of the same automated framework that we used in the 3-photon amplitude calculation [43]. Our framework performs finite-field sampling of the rational coefficients appearing in the amplitude by evaluating and combining the analytical IBP solutions from ref. [5] and the master integral solutions from ref. [49]. The analytical results for the amplitude are obtained by interpolating the finite-field samples using the library `FireFly` [51]. We refer the reader to ref. [43] for a detailed description of our framework.

3 Results

We write the finite remainder, suppressing the process (f) and helicity (\bar{h}) indices, in the following way:

$$\begin{aligned} \mathcal{F} = & Q_q^2 \mathcal{F}^{(0), Q_q^2} \left(1 + \left(\frac{\alpha_s}{4\pi} \right) \left(C_F \mathcal{R}^{(1), Q_q^2, C_F} + \frac{T_F}{C_A} \mathcal{R}^{(1), Q_q^2, T_F/C_A} + T_F \frac{Q_{l,2}}{Q_q^2} \mathcal{R}^{(1), Q_q^2, T_F} \right) \right. \\ & \left. + \left(\frac{\alpha_s}{4\pi} \right)^2 \left(N_c^2 \mathcal{R}^{(2), Q_q^2, N_c^2} + N_c n_f \mathcal{R}^{(2), Q_q^2, n_f} + n_f \frac{Q_{l,2}}{Q_q^2} \mathcal{R}^{(2), Q_q^2, n_f} \right) \right). \end{aligned} \quad (3.1)$$

In case of a vanishing tree-level amplitude we write

$$\begin{aligned} \mathcal{F} = & Q_q^2 \tilde{\mathcal{F}}^{(0), Q_q^2} \left(\left(\frac{\alpha_s}{4\pi} \right) \left(C_F \mathcal{R}^{(1), Q_q^2, C_F} + \frac{T_F}{C_A} \mathcal{R}^{(1), Q_q^2, T_F/C_A} + T_F \frac{Q_{l,2}}{Q_q^2} \mathcal{R}^{(1), Q_q^2, T_F} \right) \right. \\ & \left. + \left(\frac{\alpha_s}{4\pi} \right)^2 \left(N_c^2 \mathcal{R}^{(2), Q_q^2, N_c^2} + N_c n_f \mathcal{R}^{(2), Q_q^2, n_f} + n_f \frac{Q_{l,2}}{Q_q^2} \mathcal{R}^{(2), Q_q^2, n_f} \right) \right). \end{aligned} \quad (3.2)$$

Our fully-analytic results for the remainders $\mathcal{R}^{(\ell), i, c}$, with $\ell = 1, 2$ and i/c labelling the charge/colour structure, and for the normalisations $\mathcal{F}^{(0), Q_q^2}$ and $\tilde{\mathcal{F}}^{(0), Q_q^2}$ can be found in the supplementary material attached to this paper.

The remainders $\mathcal{R}^{(\ell),i,c}$ have the following structure:

$$\mathcal{R}^{(\ell),i,c} = \sum_e r_e^{(\ell),i,c} t_e. \quad (3.3)$$

The coefficients $r^{(\ell),i,c}$ are rational functions of s_{ij} and linear functions of tr_5 . By t_e we denote the elements of the transcendental basis. The parity-odd variable tr_5 has two distinct origins: the helicity projection and the master integrals of ref. [49]. Scalar integrals only depend on the invariants s_{ij} , however a physical phase space needs additionally the sign of $\text{Im}\{\text{tr}_5\}$ to be fully specified and this dependence is kept explicit in this master integral representation. Internally, we keep these two separate. We relabel the tr_5 originating from the masters as ε_5 and include it as part of the basis t_e . Since ε_5 only appears together with parity-odd combinations of pentagon functions, absorbing ε_5 in the transcendental basis effectively renders all elements t_e parity-even.

A comment is in order about the crossing of momenta in the presence of the parity-odd variable ε_5 and the parity-odd transcendental functions appearing in the basis of ref. [49]. When the analytic expression for a given helicity is being derived, one needs to match scalar integrals with permuted momenta to the basis t_e . In practice, these scalar integrals are the master integrals resulting from the IBP reduction of the amplitude. This matching is done in the following way. Ref. [49] provides the transcendental basis t_e indirectly, through a set of master integrals of uniform transcendentality (UTM). These UTMs depend on the invariants s_{ij} but not on ε_5 . Ref. [49] also provides for a single permutation of momenta a way of expressing a set of scalar integrals to the set of UTMs. The parity-odd variable ε_5 appears linearly in this relation. This relation allows us to map our own scalar integrals to UTMs and, from there, to t_e .

Additionally, ref. [49] provides for each UTM its complete set of permutations in all five momenta. In practice this means that we do not need to perform any crossing of momenta in the transcendental functions appearing in the basis t_e , but simply need to identify the UTMs with the correct crossing that matches the crossing of the scalar integral. The variable ε_5 , however, needs to be treated separately under permutation of momenta since it is not part of the pre-crossed set of UTMs. In particular, its sign changes under odd permutations.

When one numerically crosses momenta in a given helicity amplitude (for example, in order to derive a different helicity from a known one) the above procedure needs to be slightly modified. Since in this case one cannot rely on the set of pre-crossed UTMs anymore, one has to treat correctly the signs of both the parity-odd variable ε_5 and the parity-odd functions within the transcendental basis t_e . Specifically, if an odd permutation is involved the signs of both flip. As we previously remarked, the transcendental functions of ref. [49] allow for the numerical evaluation of crossings only if the momenta are not switched between the initial and the final states.

We have simplified the rational functions $r^{(\ell),i,c}$ appearing in the amplitudes by expressing them as linear combinations of a much smaller set of rational functions. Those have been further simplified with the help of the partial fractioning package `MultivariateApart` [52].

In the following we will be referring to this much smaller set as *independent* rational functions. The number of (independent) rational functions for each colour/charge structure can be found in table 1. The appearance of these simpler rational structures has already been discussed in the literature [37, 43–46] and they have been utilized for expressing the amplitudes in a more compact form. On the other hand, it seems to us that the possible true structure behind these independent rational functions has not yet been fully explored and we hope to return to this in a future publication.

To aid future comparisons, benchmark evaluations of the finite remainders in one kinematic point are presented in appendix A.

We have performed a number of checks on our results. When computing the 2-loop finite remainders for the two processes (2.1), we have verified that the poles in ϵ cancel. We have checked our tree-level and 1-loop results against the library `Recola` [53]. We have also verified that the dependence on tr_5 (the one originating from the projector) drops out in the spin-averaged finite remainder.

Recently, the spin-averaged amplitudes for the two processes (2.1) were calculated in ref. [44]. We have found complete agreement for all terms except for those containing ε_5 . We have investigated the origin of this discrepancy. In the process of doing this we observed that we could reproduce the results of that reference if we do not flip the sign of ε_5 under permutations during the mapping of masters to pentagon functions as well as during the numerical crossing of momenta in order to obtain all other helicities. As explained above such a treatment of ε_5 is inconsistent. In order to verify this, we have calculated the terms of order ϵ and ϵ^2 of the one-loop pentagon integral which are sensitive to the treatment of the parity-odd invariant and functions. We have verified that the calculation in terms of pentagon functions as described above agrees with a direct numerical calculation of this integral with the program `pySecDec` [54]. Our interpretation of the above result is that the disagreement between our calculation and ref. [44] is due to an inconsistent treatment in ref. [44] of ε_5 under permutations.

Note Added

After this paper was completed but before it was submitted for publication we learned that the authors of ref. [44] have independently discovered the inconsistency in the sign treatment of ε_5 mentioned above. We now find complete agreement between our results and their corrected result, which should appear in an updated version of ref. [44].

4 Conclusions

In this work we have calculated the finite remainders for the complete set of 2-loop QCD leading-colour helicity amplitudes for the processes $q\bar{q} \rightarrow g\gamma\gamma$ and $qg \rightarrow q\gamma\gamma$. The results are obtained in a compact, fully-analytical form and can be found in the supplementary material attached to this paper.

These amplitudes enable the calculation of the double-virtual QCD corrections to $\gamma\gamma j$ -production at hadron colliders. We expect that the calculation of this process in NNLO QCD

$q\bar{q} \rightarrow g\gamma\gamma$	# tot. / # ind.	$qg \rightarrow q\gamma\gamma$	# dep. / # ind.
$\mathcal{R}^{+-----,(2),Q_q^2,N_c^2}$	96 / 33	$\mathcal{R}^{+-----,(2),Q_q^2,N_c^2}$	6125 / 66
$\mathcal{R}^{+-----,(2),Q_q^2,n_f}$	48 / 22	$\mathcal{R}^{+-----,(2),Q_q^2,n_f}$	85 / 27
$\mathcal{R}^{+-----,(2),Q_q^2,n_f}$	6 / 2	$\mathcal{R}^{+-----,(2),Q_q^2,n_f}$	36 / 8
$\mathcal{R}^{+-+---,(2),Q_q^2,N_c^2}$	7266 / 66	$\mathcal{R}^{++++-,(2),Q_q^2,N_c^2}$	6200 / 101
$\mathcal{R}^{+-+---,(2),Q_q^2,n_f}$	504 / 27	$\mathcal{R}^{++++-,(2),Q_q^2,n_f}$	478 / 59
$\mathcal{R}^{+-+---,(2),Q_q^2,n_f}$	58 / 8	$\mathcal{R}^{++++-,(2),Q_q^2,n_f}$	50 / 8
$\mathcal{R}^{+---+-,(2),Q_q^2,N_c^2}$	7252 / 101	$\mathcal{R}^{++++-,(2),Q_q^2,N_c^2}$	92 / 33
$\mathcal{R}^{+---+-,(2),Q_q^2,n_f}$	736 / 59	$\mathcal{R}^{++++-,(2),Q_q^2,n_f}$	58 / 22
$\mathcal{R}^{+---+-,(2),Q_q^2,n_f}$	58 / 8	$\mathcal{R}^{++++-,(2),Q_q^2,n_f}$	4 / 2
		$\mathcal{R}^{+---+-,(2),Q_q^2,N_c^2}$	6216 / 101
		$\mathcal{R}^{+---+-,(2),Q_q^2,n_f}$	472 / 59
		$\mathcal{R}^{+---+-,(2),Q_q^2,n_f}$	50 / 8
		$\mathcal{R}^{+++++,(2),Q_q^2,N_c^2}$	6125 / 66
		$\mathcal{R}^{+++++,(2),Q_q^2,n_f}$	85 / 27
		$\mathcal{R}^{+++++,(2),Q_q^2,n_f}$	36 / 8
		$\mathcal{R}^{+----+,(2),Q_q^2,N_c^2}$	92 / 33
		$\mathcal{R}^{+----+,(2),Q_q^2,n_f}$	58 / 22
		$\mathcal{R}^{+----+,(2),Q_q^2,n_f}$	4 / 2

Table 1. Total (tot.) vs. independent (ind.) number of rational functions of the finite remainders

is achievable using the framework used in our calculation of $\gamma\gamma\gamma$ -production at the LHC [40].

In combination with the recently-calculated 3-loop QCD amplitude $q\bar{q} \rightarrow \gamma\gamma$ [48], our results open the door to the computation of the N³LO QCD corrections to $\gamma\gamma$ production.

Acknowledgments

The work of M.C. was supported by the Deutsche Forschungsgemeinschaft under grant 396021762 - TRR 257. The research of A.M. and R.P. has received funding from the European Research Council (ERC) under the European Union’s Horizon 2020 Research and Innovation Programme (grant agreement no. 683211). A.M. was also supported by the UK STFC grants ST/L002760/1 and ST/K004883/1. The research of H.C. is supported by the ERC Starting Grant 804394 HipQCD. A.M. acknowledges the use of the DiRAC Cumulus HPC facility under Grant No. PPSP226.

A Benchmark numerical results for the finite remainder

In this appendix we present numerical benchmark results for both amplitudes (2.1) evaluated at the following point

$$\mu = 1, \quad x = \{1, 43/157, 83/157, 61/157, 37/157, i\sqrt{10196683}/24649\}, \quad (\text{A.1})$$

where μ is the renormalization scale and x is defined in eq. (2.2).

In table 2 we give the values of the spin- and colour-summed squared two-loop finite reminders

$$\sum_{\bar{h}} \sum_{\text{color}} 2\text{Re} \left(\mathcal{F}^{(0)} \mathcal{F}^{(2)} \right).$$

For each amplitude we show separately the coefficients of each one of the three charge/color structures appearing in eqs. (3.1,3.2). The complete squared amplitude is then obtained by adding these three numbers each multiplied by its corresponding charge/color factor. We note that the squared amplitude is independent of the helicity conventions.

	$Q_q^2 N_c^2$	$Q_q^2 n_f$	$Q_q^2 n_f$
$q\bar{q} \rightarrow g\gamma\gamma$	156620.2	-22398.6	-1382.95
$qg \rightarrow q\gamma\gamma$	-1772.85	-564.471	4323.60

Table 2. Benchmark evaluations of the squared two loop finite remainders in the point eq. (A.1). Shown are the coefficients of the charge/color structures.

In table 3 we present the values of the coefficients $\mathcal{R}^{(2)}$ which are defined in eqs. (3.1,3.2). The reason we show these coefficients, instead of the complete two-loop finite remainders, is that the coefficients \mathcal{R} are independent of the helicity conventions. Helicities whose values are not explicitly shown are zero. As in table 2 above, the values are further split by the charge/color structures appearing in eqs. (3.1,3.2).

B Renormalisation constants

We perform the renormalisation in the $\overline{\text{MS}}$ scheme with n_f massless fermions. The UV renormalisation constant $Z_{\alpha_s} = Z_g^2$ is given by:

$$\begin{aligned} Z_g = 1 + \frac{1}{\varepsilon} \left(\frac{\alpha_s}{4\pi} \right) \frac{4n_f T_F - 11C_A}{6} + \left(\frac{\alpha_s}{4\pi} \right)^2 \left[\frac{1}{\varepsilon} \left(\frac{-17C_A^2}{6} + \frac{5C_A n_f T_F}{3} + C_F n_f T_F \right) \right. \\ \left. + \frac{1}{\varepsilon^2} \left(\frac{121C_A^2}{384} - \frac{11C_A n_f T_F}{48} + \frac{2n_f^2 T_F^2}{48} \right) \right] + \mathcal{O}(\alpha_s^3). \end{aligned} \quad (\text{B.1})$$

The IR renormalisation constant depends on the partonic process. Up to order $\mathcal{O}(\alpha_s^2)$ we find

$$\mathbf{Z}^{q\bar{q}} = 1 + \frac{\alpha_s}{4\pi} \left(\frac{\gamma_0}{2\varepsilon^2} + \frac{\Gamma_0}{2\varepsilon} \right) + \left(\frac{\alpha_s}{4\pi} \right)^2 \left(\frac{\gamma_0^2}{8\varepsilon^4} + \frac{\gamma_0(\Gamma_0 - \frac{3}{2}b_0)}{4\varepsilon^3} + \frac{\gamma_1 + \Gamma_0(\Gamma_0 - 2b_0)}{8\varepsilon^2} + \frac{\Gamma_1}{4\varepsilon} \right), \quad (\text{B.2})$$

Helicity	$\mathcal{R}^{(2),Q_q^2,N_c^2}$	$\mathcal{R}^{(2),Q_q^2,n_f}$	$\mathcal{R}^{(2),Q_{q'}^2,n_f}$
$q\bar{q} \rightarrow g\gamma\gamma$			
+- - - -	-9.0529 - 2.1449 <i>i</i>	1.8348 + 0.19391 <i>i</i>	-0.0051350 - 0.043221 <i>i</i>
-+ - - -	-9.1772 + 0.054019 <i>i</i>	1.8181 - 0.22935 <i>i</i>	0.036676 + 0.023436 <i>i</i>
-+ + + +	-9.2761 - 0.30316 <i>i</i>	1.8348 - 0.19391 <i>i</i>	-0.032907 - 0.028487 <i>i</i>
+ - + + +	-8.9122 - 2.2729 <i>i</i>	1.8181 + 0.22935 <i>i</i>	-0.0011607 + 0.043509 <i>i</i>
+ - + - -	29.541 + 2.3640 <i>i</i>	-3.3044 - 0.36765 <i>i</i>	-0.98915 - 1.3505 <i>i</i>
- + + - -	25.228 - 3.0190 <i>i</i>	-2.0349 + 0.69140 <i>i</i>	-0.67582 - 1.5260 <i>i</i>
- + - + +	30.472 - 1.4840 <i>i</i>	-3.3044 + 0.36765 <i>i</i>	-0.56354 - 1.5763 <i>i</i>
+ - - + +	24.168 + 3.2096 <i>i</i>	-2.0349 - 0.69140 <i>i</i>	-0.88457 - 1.4153 <i>i</i>
+ - - + -	27.867 + 24.401 <i>i</i>	-3.2863 - 5.2198 <i>i</i>	-0.38329 - 0.51472 <i>i</i>
+ - - - +	131.03 - 151.42 <i>i</i>	-18.442 + 33.892 <i>i</i>	-0.71375 - 2.1654 <i>i</i>
- + - + -	76.984 + 16.456 <i>i</i>	-12.948 - 1.6300 <i>i</i>	-0.39323 - 0.50343 <i>i</i>
- + - - +	-53.799 - 79.874 <i>i</i>	18.001 + 12.817 <i>i</i>	-1.3095 - 1.9617 <i>i</i>
- + + - +	72.634 + 18.963 <i>i</i>	-12.119 - 2.2083 <i>i</i>	-0.21126 - 0.60598 <i>i</i>
- + + + -	-51.989 - 89.280 <i>i</i>	17.474 + 15.070 <i>i</i>	-1.3927 - 1.8052 <i>i</i>
+ - + - +	29.848 + 27.439 <i>i</i>	-3.9115 - 5.8865 <i>i</i>	-0.19635 - 0.60788 <i>i</i>
+ - + + -	121.36 - 156.87 <i>i</i>	-16.282 + 34.746 <i>i</i>	-0.88995 - 2.1843 <i>i</i>
$qg \rightarrow q\gamma\gamma$			
+++ + -	0.55209 - 21.589 <i>i</i>	0.61496 + 6.6073 <i>i</i>	0.49135 - 3.8124 <i>i</i>
+++ - +	271.57 + 25.079 <i>i</i>	-56.389 - 8.8970 <i>i</i>	17.075 - 24.896 <i>i</i>
--- - +	-7.5468 + 7.5743 <i>i</i>	2.7324 + 0.49795 <i>i</i>	0.16991 - 2.5756 <i>i</i>
--- + -	-64.889 + 100.82 <i>i</i>	26.351 - 23.482 <i>i</i>	39.726 - 4.2734 <i>i</i>
+ - + + -	4.7570 - 72.345 <i>i</i>	-8.0046 + 16.377 <i>i</i>	6.4309 + 7.8100 <i>i</i>
+ - + - +	1.7860 - 64.731 <i>i</i>	-2.5875 + 16.314 <i>i</i>	-1.1489 - 1.8506 <i>i</i>
- + - - +	17.411 - 140.01 <i>i</i>	-9.4010 + 29.890 <i>i</i>	-1.1923 + 20.567 <i>i</i>
- + - + -	21.245 - 133.79 <i>i</i>	-12.116 + 28.169 <i>i</i>	-0.45528 - 3.0363 <i>i</i>
+ - + - -	7.5129 - 120.03 <i>i</i>	-8.7572 + 26.290 <i>i</i>	1.3220 - 2.1771 <i>i</i>
- + - + +	13.107 - 92.756 <i>i</i>	-7.0224 + 20.685 <i>i</i>	1.3220 + 2.1771 <i>i</i>
++++ +	-7.3151 - 11.657 <i>i</i>	2.6393 + 3.4849 <i>i</i>	1.6828 + 1.6226 <i>i</i>
---- -	2.2900 - 38.856 <i>i</i>	-0.39700 + 9.5972 <i>i</i>	1.6828 - 1.6226 <i>i</i>
+++ - -	3.1373 + 0.084647 <i>i</i>	-0.57085 - 0.18319 <i>i</i>	-0.42571 + 0.64703 <i>i</i>
--- + +	2.4545 + 0.89149 <i>i</i>	-0.53179 - 0.29430 <i>i</i>	-0.42571 - 0.64703 <i>i</i>
+ - + + +	-1.9218 + 1.5696 <i>i</i>	0.53536 - 0.44837 <i>i</i>	0.30067 - 0.71377 <i>i</i>
- + - - -	-2.9417 - 1.1496 <i>i</i>	0.39743 + 0.27087 <i>i</i>	0.30067 + 0.71377 <i>i</i>

Table 3. Benchmark evaluations of the two loop finite remainders in the point eq. (A.1).

with

$$b_0 = \frac{11C_A - 4n_f T_F}{3}, \quad (\text{B.3})$$

and with the following anomalous dimensions

$$\gamma_0 = -2(C_A + 2C_F), \quad (\text{B.4})$$

$$\gamma_1 = \frac{2}{9}(2C_F + C_A)(C_A(-67 + 18\zeta_2) + 20n_f T_F), \quad (\text{B.5})$$

$$\Gamma_0 = -(6C_F + b_0) - 2C_A(l_{\mu_{13}} + l_{\mu_{23}}) + 2(C_A - 2C_F)l_{\mu_{12}}, \quad (\text{B.6})$$

$$\begin{aligned} \Gamma_1 = \frac{1}{54} & \left(54C_F^2(-3 + 24\zeta_2) + C_A^2(-1384 + 198\zeta_2) + 8C_F T_F n_f(92 + 54\zeta_2) \right. \\ & - 2C_A(C_F(961 + 594\zeta_2) + 2T_F n_f(-128 + 18\zeta_2)) + 108(C_A^2 + 26C_A C_F - 24C_F^2)\zeta_3 \\ & \left. + 12(C_A(-67 + 18\zeta_2) + 20n_f T_F)(C_A(l_{\mu_{13}} + l_{\mu_{23}}) - (C_A - 2C_F)l_{\mu_{12}}) \right). \quad (\text{B.7}) \end{aligned}$$

In the above equations we have introduced the following notation: $l_{\mu_{12}} = \log(-\mu^2/s_{12})$, $l_{\mu_{23}} = \log(\mu^2/s_{23})$, and $l_{\mu_{13}} = \log(\mu^2/s_{13})$.

The factor $\mathbf{Z}^{q\bar{q}}$ is obtained from $\mathbf{Z}^{q\bar{q}}$ by replacing $l_{\mu_{12}} \rightarrow l_{\mu_{23}}$ and $l_{\mu_{23}} \rightarrow l_{\mu_{12}}$.

References

- [1] A. von Manteuffel and R. M. Schabinger, Phys. Lett. B **744** (2015), 101-104 [arXiv:1406.4513 [hep-ph]].
- [2] T. Peraro, JHEP **12** (2016), 030 [arXiv:1608.01902 [hep-ph]].
- [3] J. Böhm, A. Georgoudis, K. J. Larsen, H. Schönemann and Y. Zhang, JHEP **09** (2018), 024 [arXiv:1805.01873 [hep-th]].
- [4] A. V. Kotikov and S. Teber, Phys. Part. Nucl. **50** (2019) no.1, 1-41 [arXiv:1805.05109 [hep-th]].
- [5] H. A. Chawdhry, M. A. Lim and A. Mitov, Phys. Rev. D **99** (2019) no.7, 076011 [arXiv:1805.09182 [hep-ph]].
- [6] J. Bosma, K. J. Larsen and Y. Zhang, PoS **LL2018** (2018), 064 [arXiv:1807.01560 [hep-th]].
- [7] T. Gehrmann, J. M. Henn and N. A. Lo Presti, JHEP **10** (2018), 103 [arXiv:1807.09812 [hep-ph]].
- [8] S. Abreu, B. Page and M. Zeng, JHEP **01** (2019), 006 [arXiv:1807.11522 [hep-th]].
- [9] D. Chicherin, T. Gehrmann, J. M. Henn, N. A. Lo Presti, V. Mitev and P. Wasser, JHEP **03** (2019), 042 [arXiv:1809.06240 [hep-ph]].
- [10] P. Mastrolia and S. Mizera, JHEP **02** (2019), 139 [arXiv:1810.03818 [hep-th]].
- [11] D. Chicherin, J. M. Henn and E. Sokatchev, JHEP **01** (2019), 179 [arXiv:1811.02560 [hep-th]].
- [12] G. Kälin, G. Mogull and A. Ochirov, JHEP **07** (2019), 120 [arXiv:1811.09604 [hep-th]].
- [13] P. Maierhöfer and J. Usovitsch, [arXiv:1812.01491 [hep-ph]].
- [14] A. Kardos, [arXiv:1812.05622 [hep-ph]].

- [15] A. V. Smirnov and F. S. Chuharev, *Comput. Phys. Commun.* **247** (2020), 106877 [arXiv:1901.07808 [hep-ph]].
- [16] H. Frellesvig, F. Gasparotto, S. Laporta, M. K. Mandal, P. Mastrolia, L. Mattiazzi and S. Mizera, *JHEP* **05** (2019), 153 [arXiv:1901.11510 [hep-ph]].
- [17] S. Caron-Huot, L. J. Dixon, F. Dulat, M. von Hippel, A. J. McLeod and G. Papathanasiou, *JHEP* **08** (2019), 016 [arXiv:1903.10890 [hep-th]].
- [18] D. Bendle, J. Böhm, W. Decker, A. Georgoudis, F. J. Pfreundt, M. Rahn, P. Wasser and Y. Zhang, *JHEP* **02** (2020), 079 [arXiv:1908.04301 [hep-th]].
- [19] C. G. Papadopoulos and C. Wever, *JHEP* **02** (2020), 112 [arXiv:1910.06275 [hep-ph]].
- [20] D. C. Dunbar, J. H. Godwin, W. B. Perkins and J. M. W. Strong, *Phys. Rev. D* **101** (2020) no.1, 016009 [arXiv:1911.06547 [hep-ph]].
- [21] T. Peraro, [arXiv:1912.03142 [hep-ph]].
- [22] X. Guan, X. Liu and Y. Q. Ma, *Chin. Phys. C* **44** (2020) no.9, 093106 [arXiv:1912.09294 [hep-ph]].
- [23] D. C. Dunbar, W. B. Perkins and J. M. W. Strong, *Phys. Rev. D* **101** (2020) no.7, 076001 [arXiv:2001.11347 [hep-ph]].
- [24] A. V. Smirnov and V. A. Smirnov, *Nucl. Phys. B* **960** (2020), 115213 [arXiv:2002.08042 [hep-ph]].
- [25] J. Usovitsch, [arXiv:2002.08173 [hep-ph]].
- [26] C. Anastasiou, R. Haindl, G. Sterman, Z. Yang and M. Zeng, [arXiv:2008.12293 [hep-ph]].
- [27] S. Abreu, J. Dormans, F. Febres Cordero, H. Ita, M. Kraus, B. Page, E. Pascual, Ruf and V. Sotnikov, [arXiv:2009.11957 [hep-ph]].
- [28] D. D. Canko, C. G. Papadopoulos and N. Syrrakos, *JHEP* **01** (2021), 199 [arXiv:2009.13917 [hep-ph]].
- [29] D. Bendle, J. Boehm, W. Decker, A. Georgoudis, F. J. Pfreundt, M. Rahn and Y. Zhang, [arXiv:2010.06895 [hep-th]].
- [30] L. J. Dixon, A. J. McLeod and M. Wilhelm, [arXiv:2012.12286 [hep-th]].
- [31] S. Abreu, F. Febres Cordero, H. Ita, B. Page and M. Zeng, *PoS LL2018* (2018), 016 [arXiv:1807.09447 [hep-ph]].
- [32] S. Badger, C. Brønnum-Hansen, T. Gehrmann, H. B. Hartanto, J. Henn, N. A. Lo Presti and T. Peraro, *PoS LL2018* (2018), 006 [arXiv:1807.09709 [hep-ph]].
- [33] S. Abreu, F. Febres Cordero, H. Ita, B. Page and V. Sotnikov, *JHEP* **11** (2018), 116 [arXiv:1809.09067 [hep-ph]].
- [34] S. Badger, C. Brønnum-Hansen, H. B. Hartanto and T. Peraro, *JHEP* **01** (2019), 186 [arXiv:1811.11699 [hep-ph]].
- [35] S. Abreu, J. Dormans, F. Febres Cordero, H. Ita and B. Page, *Phys. Rev. Lett.* **122** (2019) no.8, 082002 [arXiv:1812.04586 [hep-ph]].

- [36] D. Chicherin, T. Gehrmann, J. M. Henn, P. Wasser, Y. Zhang and S. Zoia, *JHEP* **03** (2019), 115 [arXiv:1901.05932 [hep-th]].
- [37] S. Abreu, J. Dormans, F. Febres Cordero, H. Ita, B. Page and V. Sotnikov, *JHEP* **05** (2019), 084 [arXiv:1904.00945 [hep-ph]].
- [38] S. Badger, D. Chicherin, T. Gehrmann, G. Heinrich, J. M. Henn, T. Peraro, P. Wasser, Y. Zhang and S. Zoia, *Phys. Rev. Lett.* **123** (2019) no.7, 071601 [arXiv:1905.03733 [hep-ph]].
- [39] H. B. Hartanto, S. Badger, C. Brønnum-Hansen and T. Peraro, *JHEP* **09** (2019), 119 [arXiv:1906.11862 [hep-ph]].
- [40] H. A. Chawdhry, M. L. Czakon, A. Mitov and R. Poncelet, *JHEP* **02** (2020), 057 [arXiv:1911.00479 [hep-ph]].
- [41] G. De Laurentis and D. Maître, *JHEP* **02** (2021), 016 [arXiv:2010.14525 [hep-ph]].
- [42] S. Abreu, B. Page, E. Pascual and V. Sotnikov, *JHEP* **21** (2020), 078 [arXiv:2010.15834 [hep-ph]].
- [43] H. A. Chawdhry, M. Czakon, A. Mitov and R. Poncelet, [arXiv:2012.13553 [hep-ph]].
- [44] B. Agarwal, F. Buccioni, A. von Manteuffel and L. Tancredi, [arXiv:2102.01820 [hep-ph]].
- [45] S. Badger, H. B. Hartanto and S. Zoia, [arXiv:2102.02516 [hep-ph]].
- [46] S. Abreu, F. F. Cordero, H. Ita, B. Page and V. Sotnikov, [arXiv:2102.13609 [hep-ph]].
- [47] S. Kallweit, V. Sotnikov and M. Wiesemann, *Phys. Lett. B* **812** (2021), 136013 [arXiv:2010.04681 [hep-ph]].
- [48] F. Caola, A. von Manteuffel and L. Tancredi, [arXiv:2011.13946 [hep-ph]].
- [49] D. Chicherin and V. Sotnikov, *JHEP* **12** (2020), 167 [arXiv:2009.07803 [hep-ph]].
- [50] L. Chen, [arXiv:1904.00705 [hep-ph]].
- [51] J. Klappert, S. Y. Klein and F. Lange, [arXiv:2004.01463 [cs.MS]].
- [52] M. Heller and A. von Manteuffel, [arXiv:2101.08283 [cs.SC]].
- [53] S. Actis, A. Denner, L. Hofer, J. N. Lang, A. Scharf and S. Uccirati, *Comput. Phys. Commun.* **214** (2017), 140-173 [arXiv:1605.01090 [hep-ph]].
- [54] S. Borowka, G. Heinrich, S. Jahn, S. P. Jones, M. Kerner, J. Schlenk and T. Zirke, *Comput. Phys. Commun.* **222**, 313-326 (2018) [arXiv:1703.09692 [hep-ph]].